












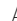





Black hole spectroscopy for precessing binary black hole coalescences

Hengrui Zhu ^{1,2,*}, Harrison Siegel ^{3,4,†}, Keefe Mitman ^{5,‡}, Maximiliano Isi ⁴, Will M. Farr ^{4,6},
Michael Boyle ⁷, Nils Deppe ^{7,8}, Lawrence E. Kidder ⁷, Sizheng Ma ⁹,
Jordan Moxon ⁵, Kyle C. Nelli ⁵, Harald P. Pfeiffer ¹⁰, Mark A. Scheel ⁵,
Saul A. Teukolsky ^{5,7}, William Throwe ⁷, Vijay Varma ¹¹ and Nils L. Vu ⁵

¹*Department of Physics, Princeton University, Jadwin Hall, Washington Road, New Jersey, 08544, USA*

²*Princeton Gravity Initiative, Princeton University, Princeton, New Jersey, 08544, USA*

³*Department of Physics, Columbia University, 704 Pupin Hall, 538 West 120th Street, New York, New York 10027, USA*

⁴*Center for Computational Astrophysics, Flatiron Institute, New York NY 10010, USA*

⁵*Theoretical Astrophysics, Walter Burke Institute for Theoretical Physics, California Institute of Technology, Pasadena, California 91125, USA*

⁶*Department of Physics and Astronomy, Stony Brook University, Stony Brook NY 11794, USA*

⁷*Cornell Center for Astrophysics and Planetary Science, Cornell University, Ithaca, New York 14853, USA*

⁸*Department of Physics, Cornell University, Ithaca, NY, 14853, USA*

⁹*Perimeter Institute for Theoretical Physics, 31 Caroline Street North, Waterloo, Ontario NSL 2Y5, Canada*

¹⁰*Max Planck Institute for Gravitational Physics (Albert Einstein Institute), Am Mühlenberg 1, D-14476 Potsdam, Germany*

¹¹*Department of Mathematics, Center for Scientific Computing and Data Science Research, University of Massachusetts, Dartmouth, MA 02747, USA*

The spectroscopic study of black hole quasinormal modes in gravitational-wave ringdown observations is hindered by our ignorance of which modes should dominate astrophysical signals for different binary configurations, limiting tests of general relativity and astrophysics. In this work, we present a description of the quasinormal modes that are excited in the ringdowns of comparable mass, quasi-circular precessing binary black hole coalescences—a key region of parameter space that has yet to be fully explored within the framework of black hole spectroscopy. We suggest that the remnant perturbation for precessing and non-precessing systems is approximately the same up to a rotation, which implies that the relative amplitudes of the quasinormal modes in both systems are also related by a rotation. We present evidence for this by analyzing an extensive catalog of numerical relativity simulations. Additional structure in the amplitudes is connected to the system’s kick velocity and other asymmetries in the orbital dynamics. We find that the ringdowns of precessing systems need not be dominated by the $(\ell, m) = (2, \pm 2)$ quasinormal modes, and that instead the $(2, \pm 1)$ or $(2, 0)$ quasinormal modes can dominate. Our results are consistent with a ringdown analysis of the LIGO-Virgo gravitational wave signal GW190521, and may also help in understanding phenomenological inspiral-merger-ringdown waveform model systematics.

I. INTRODUCTION

According to general relativity, the coalescence of two black holes results in the formation of a perturbed remnant, which equilibrates to a Kerr black hole by emitting gravitational waves in a process called the ringdown [1–3]. Ringdown emission can in general consist of a transient burst that is succeeded by a spectrum of quasinormal modes (QNMs), which then themselves decay to reveal a power-law tail [4, 5]. The QNMs are exponentially damped sinusoids with complex frequencies that are uniquely determined by the mass and spin of the remnant black hole [1, 6–10] and complex amplitudes that are nontrivially related to the initial conditions of the system [11, 12].

Much remains to be understood about how the progenitor properties of coalescing black holes map to the QNMs radiated by the remnant black hole. Numerical relativity (NR) studies of the ringdowns of comparable mass

quasi-circular binary black hole coalescences have largely been confined to non-precessing systems, where the black hole spins are perpendicular to the orbital plane. These studies have shown empirically that some progenitor information, such as the mass ratio and spin magnitudes, is encoded in the QNM amplitudes [13–19].

For precessing systems [20–23], where the progenitor black holes possess spin components parallel to the orbital plane, the picture becomes more complicated. In the extreme mass-ratio case, the relative amplitude ratios between QNMs are dictated by the spin magnitude of the heavier black hole and a small number of orbital parameters [24–27], which could be related to the connection between geodesics and QNMs in the eikonal limit [28–32]. For comparable mass systems, waveform models exist which map non-precessing waveforms to precessing ones through a time-dependent, non-inertial frame rotation to the co-precessing frame [23, 33–36], and these mappings have been extended to ringdown waveform modeling in, e.g., Refs. [34, 37–40]. Studies of the mismatch between NR waveforms and explicit QNM models, building on Ref. [41], have also been performed for precessing systems [42].

In this work, we analyze the ringdowns of precessing

* hengrui.zhu@princeton.edu

† hs3152@columbia.edu

‡ kmitman@caltech.edu

black hole binaries and present a description of QNM excitations from the perspective of observational black hole spectroscopy and perturbation theory. We fit the amplitude of each individual QNM in the canonical frame for perturbation theory—the superrest frame of the remnant [43–46]. This means that any large amplitudes we recover will correspond to large contributions of the associated modes’ frequencies in LIGO-Virgo-KAGRA [47–49] data. We analyze the ringdown within 250 NR simulations of both precessing and non-precessing binary black hole coalescences [50].

We argue that the remnant perturbations in both precessing and non-precessing systems share approximately the same geometry, but not the same orientation, and thus the amplitudes of QNMs in precessing systems are related to those of non-precessing systems by a static rotation. The angle of this rotation is determined by the misalignment of the total angular momentum flux $d\mathbf{J}/dt$ near the time of merger with the final spin χ_f of the remnant black hole. Because precessing systems can also have asymmetric inspiral emission on either side of the orbital plane, there should also be further structure in the QNM amplitudes related to properties of the system’s kick velocity [27].

We show that in some precessing systems, the dominant QNM will *not* be an $(\ell, m) = (2, \pm 2)$ QNM, but rather the $(2, \pm 1)$ or $(2, 0)$ QNMs. We also find that the precession-induced asymmetry in the gravitational wave emission can, in extreme cases, result in $\mathcal{O}(10)$ amplitude differences between $\pm m$ modes which share the same frequency. Our findings have broad implications for the interpretation of ringdown signals in data from LIGO-Virgo-KAGRA and future detectors, and may also inform investigations into the nonlinear aspects of the ringdown. Furthermore, our work provides insight into how systematic errors may arise in current phenomenological inspiral-merger-ringdown (IMR) waveform models [51, 52].

Our paper is organized as follows. In Sec. II, we discuss our QNM fitting procedure, and define parameters quantifying precession dynamics which we make use of throughout the paper. In Sec. III, we present our main results. In Sec. IV, we discuss how our work may provide insight into phenomenological inspiral-merger-ringdown waveform systematics. Finally, we conclude in Sec. V.

Our fitting and plotting codes, as well as an example simulation output, can be found in Ref. [53].

A. QNM Conventions

Throughout this work, we will refer to individual QNMs by four indices (p, ℓ, m, n) , following the notation in Ref. [54]. The angular structure of the QNMs is described by spheroidal harmonics with angular indices ℓ and m . The radial structure of the QNMs is denoted by the index n , and is also tied to the lifetime of the QNMs: the longest-lived $n = 0$ QNMs are referred to as fun-

damental QNMs, and faster-decaying $n > 0$ QNMs are called overtones. For a given set of (ℓ, m, n) , when $m \neq 0$, there are two distinct QNMs which are labeled by an index $p \equiv \text{sgn}(m \Re(\omega))$, where ω is the complex QNM frequency, and whose phase fronts are either co-rotating ($p = +$) or counter-rotating ($p = -$) with the black hole; solutions with $m = 0$ are azimuthally symmetric, so that there is no notion of co- vs counter-rotating fronts and the two possible signs of $\Re(\omega)$ directly encode the polarization. We define $A_{(p, \ell, m, n)}$ as the norm of the complex amplitude for a given (p, ℓ, m, n) QNM.

II. METHODS

A. Extracting Quasinormal Modes

We used simulations of 226 precessing and 24 non-precessing binary black hole coalescences, with mass ratios $q \leq 8$ and component spin magnitudes $\chi \leq 0.8$, created with the Spectral Einstein Code (SPEC) [50]. We computed the strain h and the five Weyl scalars at future null infinity using the SPECTRE code’s Cauchy-characteristic evolution (CCE) module [55–57]. With this asymptotic data, we mapped the simulated systems to the superrest frame of their remnant black hole 250M past the peak of the strain’s luminosity (where M is the total Christodoulou mass of the binary), using the BMS frame fixing procedure outlined in Ref. [45] and the code SCRI [58–61]. Consequently, each simulation has been transformed such that its remnant black hole is at rest at the origin, has its spin in the positive- \hat{z} direction, and has no Moreschi supermomentum [43–45]. This post-processing is necessary in order to robustly extract physical QNM amplitudes [44, 45].

For each simulation, we simultaneously fit the strain using a QNM model with all fundamental modes $(p, \ell, m, 0)$ for $p \in \{+, -\}$, $\ell \in \{2, 3\}$, and $m \in \{-\ell, -\ell + 1, \dots, \ell\}$. This model is fit over the two-sphere using a linear least-squares routine [16, 62, 63] and the following procedure¹:

- Fit the waveform from t_0 to $100M$ past t_{peak} , where t_0 is the start time of the fit and is evenly varied from $20M$ to $80M$, in increments of $0.5M$, past t_{peak} —note that t_{peak} is the time at which the strain’s luminosity reaches its maximum value (see Eq. (2.8) of Ref. [68]);
- Over a series of windows in t_0 with a length of $20M$, compute the fractional uncertainty for each of the QNM amplitudes;
- Compute the mean of these fractional uncertainties over the fitted QNMs;

¹ Similar fitting procedures have also been used in Refs. [64–67].

- Check to see which t_0 window has the minimum mean fractional uncertainty and use this window to extract the amplitude (as a mean over the window) of each of the QNMs in the ringdown model.

This routine ensures that the QNMs are extracted over the window of start times in which their recovered amplitudes are all, on average, the most stable. We do this rather than simply fitting at a fixed time because the timescales of the QNMs vary from system to system, depending on the magnitude of the remnant's spin. Over our entire catalog, this routine results in fits that have window start times $t - t_{\text{peak}} \approx 33M \pm 7M$ and relative errors over the two-sphere of $\sim 0.8\%$. Fitting at such late times enables us to avoid having to consider overtones and nonlinearities in our analysis. Nonetheless, for completeness we checked and confirmed that the inclusion of the first overtone for each QNM does not impact our results.

B. Precession Parameters

In addition to the QNM amplitudes, we also compute two other precession-induced quantities in the superrest frame of the remnant: the angle θ between the total angular momentum flux $d\mathbf{J}/dt$ at t_{peak} and the final remnant spin χ_f , and the angle ϕ of the remnant kick velocity \mathbf{v} with respect to χ_f . We formally define the remnant spin misalignment angle θ as

$$\theta = \cos^{-1} \left[\frac{d\mathbf{J}/dt(t = t_{\text{peak}})}{\|d\mathbf{J}/dt(t = t_{\text{peak}})\|} \cdot \frac{\chi_f}{\|\chi_f\|} \right], \quad (1)$$

where $d\mathbf{J}/dt$ is the total angular momentum flux (see Eq. (2.24) of Ref. [68]), χ_f is the spin of the remnant black hole measured at future null infinity (see Eq. (15) of Ref. [69]), and $\|\cdot\|$ is the L^2 norm. This angle shares similarities with the precession angles and optimal emission direction as identified in, e.g., Refs. [33–35, 37], but will be used here only to characterize theoretical predictions of the remnant perturbation's structure at the time of peak strain. The kick angle ϕ is given by

$$\begin{aligned} \phi &= \cos^{-1} \left[\frac{\mathbf{v}_{\text{CoM}}^{\text{remnant}} - \mathbf{v}_{\text{CoM}}^{\text{binary}}}{\|\mathbf{v}_{\text{CoM}}^{\text{remnant}} - \mathbf{v}_{\text{CoM}}^{\text{binary}}\|} \cdot \frac{\chi_f}{\|\chi_f\|} \right] \\ &= \cos^{-1} \left[-\frac{\mathbf{v}_{\text{CoM}}^{\text{binary}}}{\|\mathbf{v}_{\text{CoM}}^{\text{binary}}\|} \cdot \frac{\chi_f}{\|\chi_f\|} \right], \end{aligned} \quad (2)$$

where $\mathbf{v}_{\text{CoM}}^{\text{remnant}} = 0$ in the superrest frame of the remnant, and $\mathbf{v}_{\text{CoM}}^{\text{binary}}$ is the pre-merger center-of-mass velocity (see Eq. (12) of Ref. [69]) of the binary in the same frame. We extract the latter over a $500M$ window starting at $t = t_{\text{peak}} - 1000M$ using the procedure outlined in Ref. [45].

We make use of the Wigner-D matrices $\mathfrak{D}_{m',m}^\ell(\mathbf{R})$ that govern the mixing of spin-weighted spherical harmonics under rotations through the transformation [59, 70–72]

$${}_s Y'_{(\ell,m')} = \sum_m \mathfrak{D}_{m',m}^\ell(\mathbf{R}) {}_s Y_{(\ell,m)}, \quad (3)$$

where \mathbf{R} is some quaternion, ${}_s Y_{(\ell,m)}$ is a spin-weight s spherical harmonic, and primes indicate a rotated frame. The Wigner-D matrices mix amplitudes of harmonics with the same ℓ but different m . Because we will be strictly interested in static rotations off the \hat{z} axis by the remnant spin misalignment angle θ , we simplify our notation to

$$\mathfrak{D}_{m',m}^\ell(\mathbf{R}) \rightarrow \mathfrak{D}_{m',m}^\ell(\theta), \quad (4)$$

where now $\mathfrak{D}_{m',m}^\ell(\theta)$ represents a rotation by an angle θ off the \hat{z} axis, but not about it. If we consider co-rotating and counter-rotating perturbations, it can be shown that a fully co-rotating $+m$ perturbation, when rotated by $\theta = \pi$ off the remnant spin axis, would instead excite fully counter-rotating $-m$ modes [73].

III. RESULTS

Before delving into our results, we first provide a conceptual framework that explains the ringdown amplitudes of precessing binary black hole coalescences by characterizing the structure of the remnant perturbations.

Evidence from NR suggests that the merger stage of a comparable-mass binary black hole coalescence is generally short-lived [2, 77, 78]. This implies that the state of the binary before merger may be directly related to the structure of the remnant perturbation immediately following merger [13, 14, 17].

In linear perturbation theory, the QNMs are sourced by perturbations to a fixed Kerr background corresponding to the final remnant. In keeping with this framework, we must study the structure of the perturbation sourced by the binary in a frame aligned with the final remnant spin χ_f .

Because the dominant angular content of the inspiral emission in the co-orbital frame for precessing systems is similar to that of non-precessing systems (up to asymmetries over the orbital plane) [33, 35, 60, 72, 79], we assume the geometry (but not the orientation) of the remnant perturbation is roughly the same in both cases. We assume the total angular momentum of the perturbation is oriented along the binary orbital angular momentum \mathbf{L} as evaluated at a time near merger, e.g., t_{peak} . Because we do not have direct access to \mathbf{L} in our simulations, in practice we use the total angular momentum flux $d\mathbf{J}/dt$ which is parallel to \mathbf{L} up to 1 post-Newtonian (PN) order [21, 22].

In precessing systems, χ_f will not necessarily be parallel to \mathbf{L} . This means that, as viewed by the remnant in the χ_f -aligned frame where QNMs are defined, the perturbation is rotated by the angle θ between \mathbf{L} and χ_f . Therefore, the QNMs of a precessing system should be approximately sourced by a rotated version of the perturbation that acts on the remnant of a non-precessing system, and the QNM amplitudes of precessing and non-

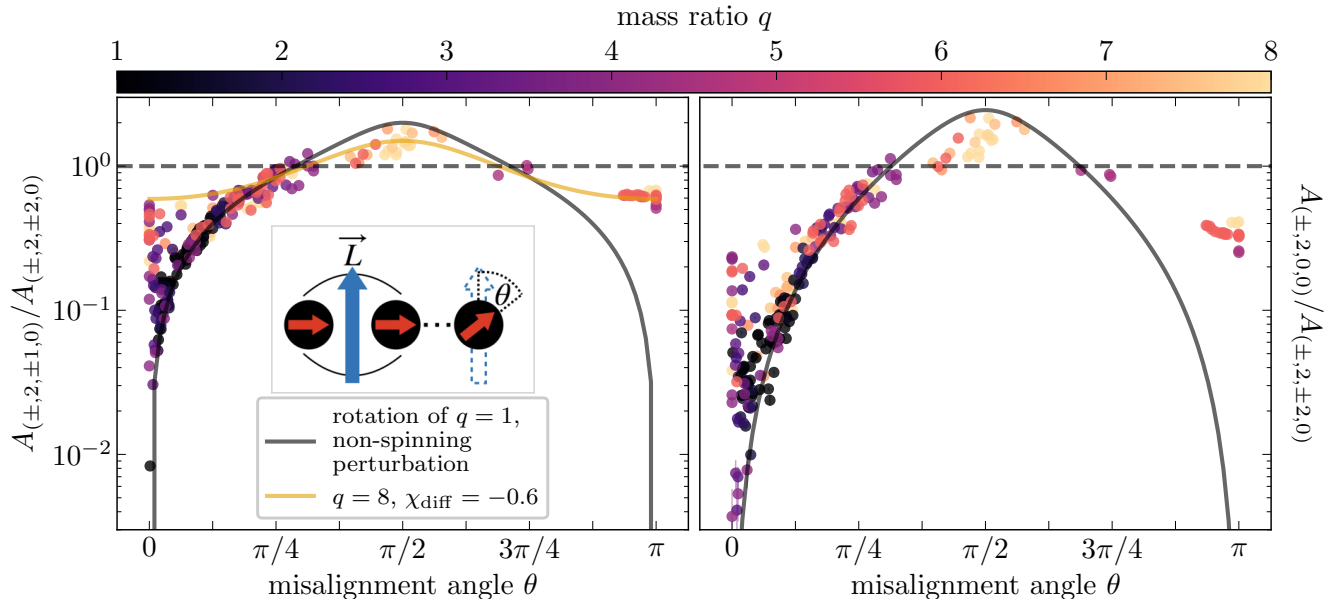


FIG. 1. *Left*: Summed amplitude ratios (see Eq. (5)) of the co-rotating and counter-rotating $(\ell, m) = (2, \pm 1)$ and $(\ell, m) = (2, \pm 2)$ fundamental QNMs, versus the remnant spin misalignment angle θ ; see Eq. (1). Color shows the binary mass ratio. One can roughly predict the QNM amplitude ratio for comparable mass precessing binaries by rotating an $(\ell, m) = (2, \pm 2)$ spherical harmonic by θ off the \hat{z} axis and taking the resulting ratio of different (ℓ, m) harmonics in the rotated frame. This prediction for $q = 1$ systems is shown as a black curve; see Eq. (6). For systems with a higher mass-ratio and non-zero spins, the $\theta = 0$ perturbation to be rotated will include significant $\ell \neq m$ content, dependent on the mass ratio and progenitor spins [13, 14, 74–76]. An example for the rotation of a $q = 8$, $\chi_{\text{diff}} = -0.6$ perturbation is shown by the yellow curve; see Eq. (10). Note that higher mass-ratio systems can have larger values of θ , since the spin of the more massive black hole can contribute a larger fraction of the remnant’s final spin in these systems. *Right*: Identical to the other panel, but for the $(2, 0)$ fundamental QNMs. Here we only show a prediction for a $q = 1$, non-spinning system because models of the $\theta = 0$ excitation of the $(2, 0)$ QNM as a function of q and χ_{diff} are not as readily available as those of the $(2, 1)$ QNM, i.e., something like Eq. (10).

precessing systems should thus be related by a simple rotation of θ at a fixed time.

Given the above conceptual picture, we can obtain an approximation for the amplitude ratios of QNMs in precessing systems by rotating the angular content of the dominant perturbation expected in a non-precessing $\theta = 0$ system. For simplicity we assume, to reasonable approximation for equal mass non-spinning binaries, that the dominant $\theta = 0$ perturbation is comprised solely of equal-amplitude co-rotating $(\ell, m) = (2, \pm 2)$ harmonics. We can also account for larger mass ratios or spins by additionally rotating odd m perturbations [13, 14]. With the aforementioned assumptions, we predict that counter-rotating QNM amplitudes are large for $\theta > \pi/2$, and $\ell \neq m$ QNM amplitudes are large for $\theta \simeq \pi/2$. As we will show below, these assumptions appear to accurately describe the behavior of precessing systems. In the case of highly spinning anti-aligned binaries, there may also be $\theta = 0$ contributions from $(\ell, m) = (2, 0)$ perturbative content, since these binary configurations cause the final state to more closely resemble a head-on collision, and in principle these contributions should also be included in our rotated-perturbation prediction; we do not cur-

rently account for such perturbative content, and leave the study of this part of parameter space for future work.

As an example, we explicitly show here how we derive our prediction for the QNM amplitude ratio $A_{(\pm,2,\pm 1,0)}/A_{(\pm,2,\pm 2,0)}$, where we have defined

$$A_{(\pm,\ell,\pm m,0)}^2 = A_{(+,\ell,m,0)}^2 + A_{(-,\ell,m,0)}^2 + A_{(+,\ell,-m,0)}^2 + A_{(-,\ell,-m,0)}^2, \quad (5)$$

i.e., the norm of a multi-dimensional amplitude vector. Our rotated-perturbation prediction is given by

$$\frac{\mathfrak{D}_{1,2}^{\ell,\pm}(\theta, q, \chi_{\text{diff}})}{\mathfrak{D}_{2,2}^{\ell,\pm}(\theta, q, \chi_{\text{diff}})}, \quad (6)$$

where

$$\left[\mathfrak{D}_{m_1, m_2}^{\ell,\pm}(\theta, q, \chi_{\text{diff}}) \right]^2 = \left[\frac{A_{(\ell, m_1)}}{A_{(\ell, m_2)}}(q, \chi_{\text{diff}}) \mathfrak{D}_{m_1, m_1}^{\ell,\pm}(\theta) \right]^2 + \left[\mathfrak{D}_{m_1, m_2}^{\ell,\pm}(\theta) \right]^2, \quad (7)$$

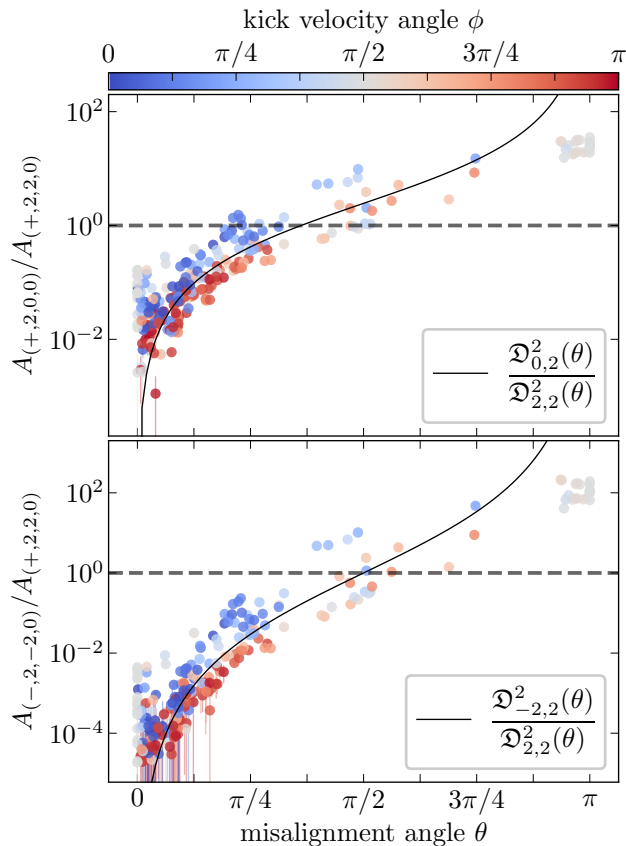


FIG. 2. *Top*: Amplitude ratio of the co-rotating $(+, 2, 0, 0)$ and $(+, 2, 2, 0)$ fundamental QNMs, versus the remnant spin misalignment angle θ ; see Eq. (1). Color shows the angle between the kick velocity and the remnant spin direction; see Eq. (2). The black curve is the prediction for this amplitude ratio based on the rotation of spin-weighted spherical harmonics assuming $q = 1$ and a non-spinning binary. *Bottom*: Identical to the top panel, but for the counter-rotating $(-, 2, -2, 0)$ and co-rotating $(+, 2, 2, 0)$ fundamental QNMs. Note for $\theta \gtrsim \pi/2$ the counter-rotating QNMs dominate [37]. Fractional uncertainties here are larger, since the absolute values of the counter-rotating amplitudes are close to zero for small values of θ .

with

$$\left[\mathfrak{D}_{m'_1, m_2}^{\ell, \pm}(\theta)\right]^2 = \left[\mathfrak{D}_{m'_1, m_2}^{\ell}(\theta)\right]^2 + \left[\mathfrak{D}_{-m'_1, m_2}^{\ell}(\theta)\right]^2 \quad (8)$$

and

$$\chi_{\text{diff}} = \frac{q}{1+q}\chi_1 - \frac{\chi_1 + \chi_2}{2(1+q)}. \quad (9)$$

For the ratio of perturbative $A_{(2,1)}/A_{(2,2)}$ content to rotate by θ in Eq. 7, we use the result of Ref [13] for spin-aligned binaries, i.e.,

$$A_{(2,1)}/A_{(2,2)} \approx |0.43(\sqrt{1-4\nu} - \chi_{\text{diff}})|, \quad (10)$$

where

$$\nu = \frac{q}{(1+q)^2}. \quad (11)$$

In Fig. 1, we show that this rotated-perturbation prediction tracks $\ell = 2$ fundamental QNM amplitude ratios well as a function of θ . Notably, we observe that for $\theta \simeq \pi/2$, the most dominant QNMs in comparable mass precessing systems will *not* be the co-rotating or counter-rotating $(\ell, m) = (2, \pm 2)$ QNMs, as is often assumed in spectroscopic tests, but rather the $(2, \pm 1)$ (left) or the $(2, 0)$ QNMs (right). Even in cases where the $(2, \pm 2)$ QNMs are intrinsically dominant when measured over the entire celestial sphere as we do here, precession-amplified $\ell \neq m$ QNMs can still appear dominant in observational data due to viewing angle effects and thus may play a significant role in observational black hole spectroscopy.

Despite overall good agreement, our data does have some spread around our theoretical prediction. Precessing systems exhibit asymmetries in their inspiral emission above and below the orbital plane. The asymmetries of the binary can be passed on to the perturbations of the remnant to create differences in the amplitudes of the $\pm m$ QNMs [19, 27, 80]. This is partly responsible for the spread around our rotated-perturbation prediction in Fig. 1. Asymmetric emission is associated with nonzero remnant kick velocities [61, 81–87]. In Fig. 2 we show how the kick direction leaves imprints on the ringdown which neatly correspond to deviations from our rotated-perturbation predictions. It might be possible to model such effects by using additional PN information, as in Ref. [17] for example; we save this for future work.

In the top panel of Fig. 2 we compare the kick direction with spreads around our rotated-perturbation prediction for $A_{(+,2,0,0)}/A_{(+,2,2,0)}$; examining only one sign of m should make us more sensitive to hemispheric asymmetries. For $\theta \lesssim \pi/4$, where the $(\ell, m) = (2, \pm 2)$ modes dominate, we find that the spread is indeed correlated with the kick velocity's direction: a kick in the positive- \hat{z} direction corresponds to less radiated power in the $(2, 2)$ mode, while a kick in the negative- \hat{z} direction corresponds to more radiated power in the $(2, 2)$ mode. However, when $\pi/4 \lesssim \theta \lesssim 3\pi/4$, then $A_{(+,2,0,0)} \simeq A_{(+,2,2,0)}$, and the kick velocity is no longer as strongly correlated with only one $(\ell, \pm m)$ QNM.

In the bottom panel of Fig. 2, we show a similar result when comparing the counter-rotating $(-, 2, -2, 0)$ and co-rotating $(+, 2, 2, 0)$ QNM amplitudes; these amplitudes should be related as per the discussion in Sec. II. When $\theta > \pi/2$, the counter-rotating QNMs dominate over the co-rotating QNMs [37]. Again, the spread of the amplitude ratio around the rotated-perturbation prediction is in part governed by the rotated-direction of the kick velocity with respect to the remnant spin.

The spread of systems near $\theta = 0$ in Fig. 1, even for nearly equal mass systems, can also be partly attributed to asymmetric emission. Many of these systems are precessing despite having zero remnant spin misalignment, as shown in Fig. 7 in Appendix B. Most have progenitors whose spins are almost equal and opposite, meaning that the remnant spin direction is dominated by the direction of \mathbf{L} . These configurations can result in large kicks and

consequently large asymmetries in the QNM excitations.

Not only can precession induce asymmetric excitations of QNMs, but because the phases and magnitudes of the precession-induced asymmetries in the inspiral are not the same for all ℓ and m in the remnant frame, the QNM amplitude ratio $A_{(p,\ell,m,n)}/A_{(p,\ell,-m,n)}$ need not always be unity for a given ℓ and different $|m|$ in a given system. PN expansions suggest that the magnitude of asymmetry in the dominant modes during the inspiral can become $\mathcal{O}(1)$ close to merger [60]; we show in Fig. 3 that the degree of asymmetry in certain QNMs can be $\mathcal{O}(10)$ in the most extreme cases, and can be distributed in a variety of ways, presumably based on the orbital phase and the particular spin configuration of each system. Note that these extreme cases of asymmetry emerge in systems which are astrophysically plausible. As a result of emission asymmetries, precessing systems can produce radically different observable QNM amplitude spectra depending on the viewing angle of any terrestrial detectors.

Lastly, we demonstrate that our conceptual picture seems to naturally extend to $\ell = 3$ modes, and likely applies to higher ℓ as well. For non-equal mass non-precessing systems, the $(3, 3)$ mode typically dominates over the $(3, 2)$ mode [13]; thus we will assume that we can predict the $\ell = 3$ QNM amplitudes of precessing systems by rotating a $(3, \pm 3)$ co-rotating perturbation by θ . In Fig. 4, we show that the relative amplitudes between the co-rotating $\ell = 3$, $m < 3$ fundamental QNMs and the $(+, 3, 3, 0)$ QNM follow this prediction. However, the spread around the prediction is no longer as clearly explained by the kick velocity angle ϕ , because these modes are not as centrally tied to the kick direction due to their subdominant amplitudes.

IV. IMPLICATIONS FOR IMR WAVEFORM MODELS

Our work may be used to help improve phenomenological IMR waveform models. As one example, we consider here the frame in which many IMR waveform models fit the ringdown, and how our work may provide insights into systematic biases associated with methods used to transform into this frame.

Phenomenological IMR waveform models for precessing binary black hole coalescences are often constructed in a non-inertial co-precessing frame, since this simplifies the angular harmonic mode decomposition [33, 72, 79]. During the ringdown, many of these models track the time-dependent Euler angles (α, β, γ) of the co-precessing frame using the following assumption for $\dot{\alpha}$ and $\dot{\beta}$ [34]:

$$\begin{aligned}\dot{\alpha} &= \Re(\omega_{220} - \omega_{210}) \\ \dot{\beta} &= \Im(\omega_{220} - \omega_{210}),\end{aligned}\quad (12)$$

where the complex ω_{lmn} frequencies correspond to co-rotating QNMs, unless the misalignment angle θ (or roughly equivalently β , as in waveform modeling liter-

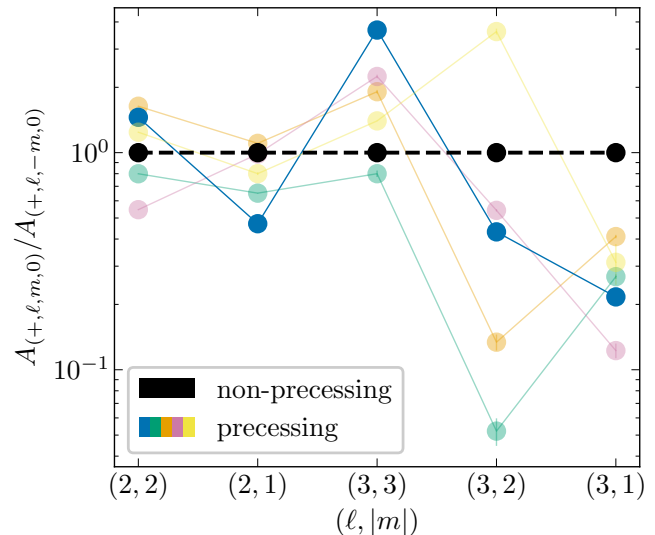


FIG. 3. Amplitude ratio of co-rotating $\pm m$ QNMs, using a small subset of simulations in our catalog (see table below; order matches the order of the legend). Each color denotes a fit from an individual simulation. In precessing systems there are asymmetries in the emission power above and below the orbital plane, which are correlated with asymmetries in the QNM amplitudes over the remnant equatorial plane. The asymmetries for given ℓ and $|m|$ harmonics can be large, $\mathcal{O}(10)$ in the extreme cases shown here, and distributed in diverse ways for different systems. Errors in the amplitude ratios are mostly too small to be seen.

ID [53]	q	$\vec{\chi}_1$	$\vec{\chi}_2$
115	1.5	(-0.55, +0.41, -0.41)	(+0.29, -0.32, -0.48)
124	1.2	(+0.14, -0.51, +0.39)	(+0.32, +0.67, -0.21)
96	1.0	(-0.73, -0.34, +0.01)	(-0.35, -0.38, +0.61)
97	1.0	(+0.07, +0.80, -0.01)	(-0.29, -0.45, +0.59)
162	3.4	(+0.19, -0.11, +0.75)	(+0.33, +0.60, -0.12)

ature) is greater than $\pi/2$ in which case the counter-rotating QNM frequencies are often used instead. For $\dot{\gamma}$, many models use the “minimal rotation condition” [35],

$$\dot{\gamma} = -\dot{\alpha} \cos(\beta). \quad (13)$$

As discussed in Ref. [34], Eq. (12) is only a good approximation when the $(\ell, m) = (2, 0)$ QNM amplitude in the remnant frame is zero. However, as we show in Fig. 1, the $(2, 0)$ QNM can be strongly excited for systems with a large misalignment angle. Thus, Eq. (12) may be a source of systematic error in many waveform models: as the $(2, 0)$ QNMs are more and more excited, Eq. (12) becomes less and less accurate. Note that Eq. (12) also assumes that the Euler angles evolve monotonically; however, there will in general be oscillations in the Euler angles due to the angular structure of the spheroidal harmonics and the beating of different modes off of each other (for evidence of this beating, see, e.g., Fig. 14 of Ref. [88]).

In Fig. 5, we provide empirical evidence of how Eq. (12)

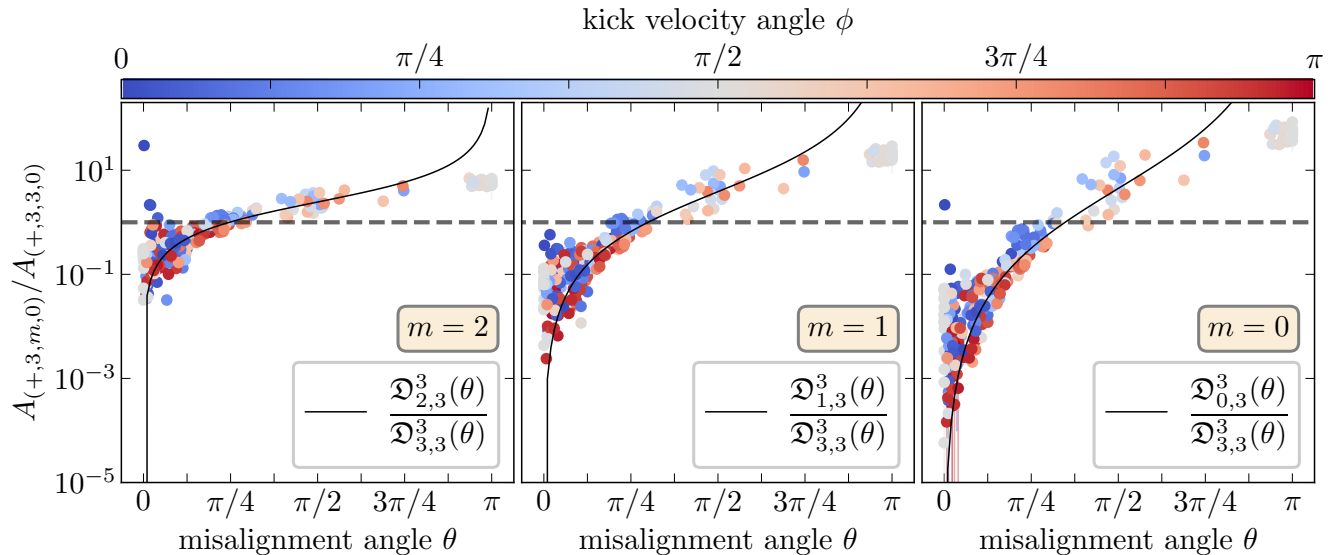


FIG. 4. Amplitude ratio between co-rotating (3,2), (3,1), (3,0), and the (3,3) fundamental QNMs. The rotated-perturbation predictions (black curves) are obtained by rotating a $(3, \pm 3)$ spherical harmonic by θ , i.e., by implicitly assuming that the dominant perturbation for $\theta = 0$ consists solely of co-rotating $(3, \pm 3)$ content. Because our catalog mostly contains $q \neq 1$ precessing simulations, this assumption is reasonable. The kick velocity is not as straightforwardly correlated with $\ell = 3$ QNM amplitudes as it is with $\ell = 2$ QNM amplitudes (see Fig. 2).

may lead to systematic bias, especially for highly precessing and more unequal mass ratio signals. On the vertical axis, we show the mismatch \mathcal{M} between waveforms $h_{\text{exact}}^{\text{coprec.}}$ and $h_{\text{Euler angle approx.}}^{\text{coprec.}}$, which are respectively mapped to a co-precessing frame over the time interval $[0M, 100M]$ by either exactly tracking the optimal emission direction using the technique presented in Ref. [59], or using Eqs. (12) and (13). We define the mismatch as

$$\mathcal{M}(h_1, h_2)|_{t_0}^{t_f} \equiv 1 - \frac{O(h_1, h_2)}{\sqrt{O(h_1, h_1)O(h_2, h_2)}}, \quad (14)$$

where

$$O(h_1, h_2) \equiv \int_{t_0}^{t_f} \int_{S^2} h_1 \overline{h_2} d\Omega dt. \quad (15)$$

As expected, as the misalignment angle θ increases, the mismatch between the two differently transformed waveforms increases, approaching $\mathcal{O}(10^{-1})$ in regions of parameter space where the $(\ell, m) = (2, 0)$ QNMs dominate. Note that the systems with $\theta \sim \pi$ also generally exhibit large mismatches because their more unequal mass ratios can allow for more fine-tuned polarizations and they can simultaneously excite more modes, which increases the complexity of their optimal emission direction's time dependence.

To our knowledge, Eq. (12) is used in the following IMR waveform models, although we note that this list may not be exhaustive:

- TEOBResumS: Eq. (21) in Ref. [89]

- SEOBNRv4PHM: Eq. (3.4) in Ref. [90]
- SEOBNRv5PHM: Eqs. (18) – (22) in Ref. [91], via the term ω_{prec}
- IMRPhenomTPHM: Eq. (24) in Ref. [92]
- Hamilton *et al.* (Ref. [37]): Eqs. (9) – 10, Eqs. (13) – (15), and Eq. (35), although they also make use of NR tuning to the frequencies of some of the dominant modes.
- IMRPhenomXO4A [93], IMRPhenomPNR [94]: Both use Ref. [37], and thus indirectly use Eq. (12)
- Marsat and Baker (Ref. [88]): Eqs. (95) – (96).

Generally, when there are multiple options implemented for describing the ringdown co-precessing frame Euler angles α and β in one of the above models, Eq. (12) is the default.

A model which explicitly fits QNMs, such as Ref. [95], might benefit from incorporating our simple rotated-perturbation prediction for the individual QNM amplitudes.

V. CONCLUSION

By fitting the first-order fundamental quasinormal mode amplitudes in the ringdowns of 250 numerical relativity simulations of both non-precessing and precessing binary black hole coalescences, we demonstrate in this

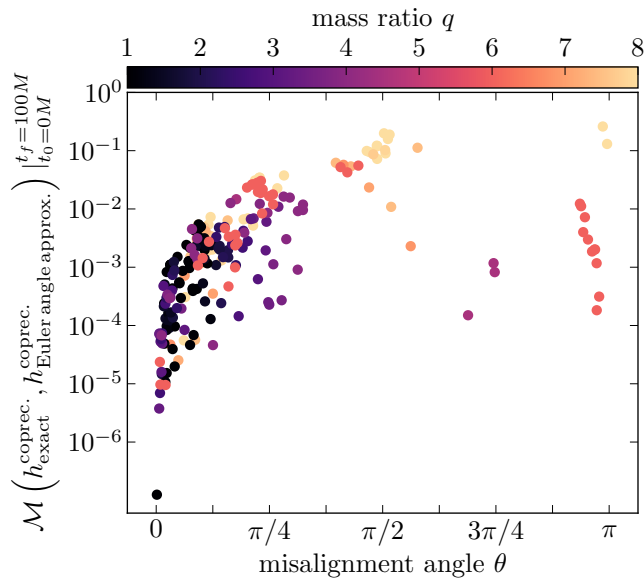


FIG. 5. Systematic error associated with the co-processing frame prescription for the ringdown Euler angles of Eq. (12). This prescription is incorporated in many phenomenological IMR waveform models, and breaks down if the $(\ell, m) = (2, 0)$ QNMs are excited; as we show in Fig. 1, the $(2, 0)$ QNMs are excited in many precessing configurations, and thus Eq. (12) may be a source of systematic error that affects current and future data analyses. On the horizontal axis we show the misalignment angle θ . On the vertical axis, we show the mismatch (see Eq. (14)) between co-processing frame waveforms obtained by mapping from the system’s inertial waveform using two different methods: (1) exactly tracking the direction of maximal emission [59], or (2) using Eqs. (12) and (13). Only precessing systems are shown. As the misalignment angle increases and the $(2, 0)$ modes become relatively more excited, the mismatch increases due to the inaccuracy of Eq. (12). Note that for $\theta \geq \pi/2$, we replace the co-rotating frequencies in Eq. (12) with counter-rotating frequencies which have opposite-sign real components.

work that the remnant perturbations in precessing systems are related to those of non-precessing systems by a static rotation of the ringdown perturbation. We characterize this rotation by the misalignment of two quantities: the total angular momentum flux $d\mathbf{J}/dt$ near the time of merger and the final spin χ_f of the remnant black hole.

We show that in some precessing systems the dominant quasinormal mode will *not* be an $(\ell, m) = (2, \pm 2)$ quasinormal mode, but rather an $(\ell, m) = (2, \pm 1)$ or an $(\ell, m) = (2, 0)$ quasinormal mode, contrary to what is commonly assumed in ringdown analyses of LIGO-Virgo-KAGRA data [96–112]. Additionally, precession-induced emission asymmetries, which are correlated with remnant kicks and other orbital dynamics, are encoded in the quasinormal mode spectra. These asymmetries can be large, such that amplitude ratios of individual $\pm m$ quasinormal modes which share the same frequency can be $\mathcal{O}(10)$ in some precessing systems. This implies that,

for real measurements, the viewing angle can alter the observed quasinormal mode amplitudes of a precessing system more than would be possible in a non-precessing system.

Crucially, the excitation of $\ell \neq |m|$ modes does not arise from operating in a non-inertial frame, as our fitting is performed in the superrest frame of the remnant, i.e., the inertial frame in which quasinormal modes are defined by perturbation theory. Our fits return the amplitude attached to the specific frequency of a physical (p, ℓ, m, n) quasinormal mode. This means that any large amplitudes we recover will correspond to large contributions of those associated frequencies in observed LIGO-Virgo-KAGRA data, which must be taken into account in order to accurately perform black hole spectroscopy.

Our results are consistent with a recent analysis [113] of the LIGO-Virgo gravitational wave signal GW190521_030229 [114], wherein ringdown models with a large $(\ell, |m|) = (2, 1)$ fundamental quasinormal mode amplitude were found to produce remnant mass and spin estimates in agreement with those of NRSur7dq4 [115].² Furthermore, our results are similar to Ref. [26], where it was found that the excitation of quasinormal modes in extreme mass-ratio systems is correlated with the polar angle of plunge of the smaller mass. The conceptual picture presented in our work may be valid over all binary mass ratios.

Our work may also help improve understanding of systematic biases in phenomenological inspiral-merger-ringdown waveforms [51, 52]. We have shown that our work highlights where a common assumption [34] regarding the co-processing frame optimal emission direction in these waveform models breaks down. We also note that a model which explicitly fits QNMs, such as Ref. [95], might benefit from incorporating our simple rotated-perturbation prediction for the individual QNM amplitudes.

One might think that at times immediately following the peak strain, the rapidly changing emission direction of precessing systems might preclude the application of perturbation theory [94]. Our work suggests however that, at least to linear order in perturbation theory, information from the point of peak luminosity imprints itself on the ringdown of a precessing system in a straightforward way.

VI. ACKNOWLEDGEMENTS

We thank Katerina Chatziioannou, Scott Hughes, Yuri Levin, Frans Pretorius, and Aaron Zimmerman for valuable conversations. We are also grateful to Eleanor Hamilton, Mark Hannam, Sascha Husa, Lionel London,

² An alternative interpretation of this signal was originally put forth in Ref. [111], and replicated and commented on at length in Ref. [113].

Geraint Pratten, and Antoni Ramos-Buades for their insight on this work in the context of gravitational waveform modeling. Computations for this work were performed with the Wheeler cluster at Caltech. This work was supported in part by the Sherman Fairchild Foundation and NSF Grants No. PHY-2011968, PHY-2011961, PHY-2309211, PHY-2309231, OAC-2209656 at Caltech., as well as NSF Grants No. PHY-2207342 and OAC-2209655 at Cornell. V.V. acknowledges support from NSF Grant No. PHY-2309301. The Flatiron Institute is a division of the Simons Foundation. H.S.’s research is supported by Yuri Levin’s Simons Investigator Award 827103. *Software:* SEABORN [116], MATPLOTLIB [117], JUPYTER [118], NUMPY [119], PYTHON3 [120].

APPENDICES

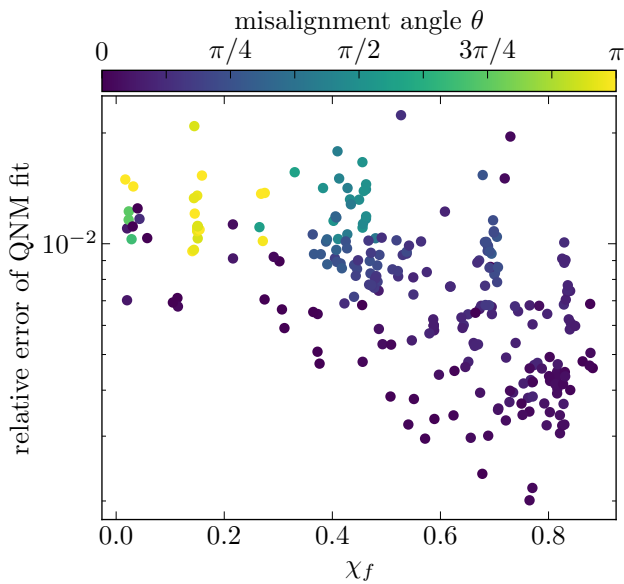


FIG. 6. Relative error of QNM fit, versus the remnant spin, colored by the misalignment angle θ . We find that the relative error decreases with increasing spin, as the QNMs are longer-lived. Precessing binaries in our catalog in general yield remnant spins smaller than the non-precessing systems, thereby resulting in higher error, but the relative error remains on the order of 1%.

Appendix A: Error of QNM fits

To characterize the quality of the QNM fits, we define the following fitting error:

$$E(t_0) \equiv \sum_{\ell \in \{2,3\}} \sum_{|m| \leq \ell} \frac{\int_{t_0}^{100M} |h_{(\ell,m)} - h_{(\ell,m)}^{\text{QNMmodel}}|^2 dt}{\int_{t_0}^{100M} |h_{(\ell,m)}|^2 dt} \quad (\text{A1})$$

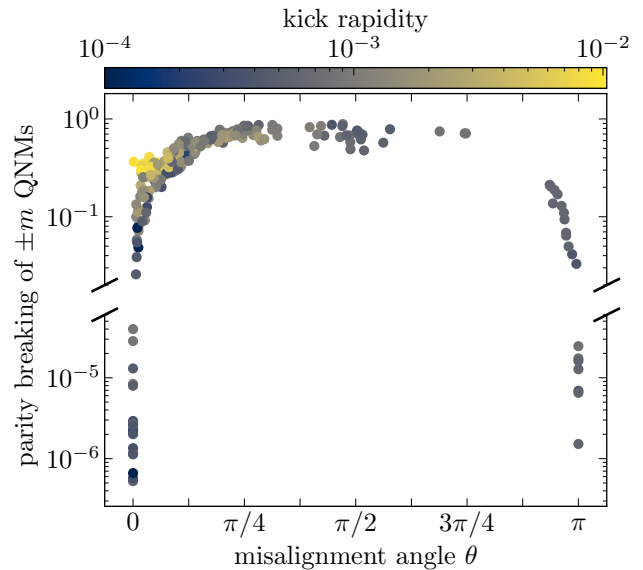


FIG. 7. Parity breaking of $\pm m$ QNMs over the remnant equator as computed via Eq. (B2), versus the misalignment angle θ . Non-precessing systems maintain reflection symmetry over the remnant equator in the ringdown, whereas precessing systems do not: here the events with small asymmetries (below the vertical axis break) are non-precessing. Note that many precessing systems have $\theta \approx 0$ or π , i.e., remnant spin misalignment is not necessitated by precession. Especially at $\theta \approx 0$, many precessing systems are characterized by large kick rapidities: many of these systems have roughly equal component spins fully anti-aligned with each other [83], and thus the total angular momentum of the binary and subsequently the spin of the remnant is dominated by \mathbf{L} .

In Fig. 6, we plot the mean of $E(t_0)$ over the most stable window of each simulation versus the magnitude of the remnant’s spin, colored by the misalignment angle θ . As can be seen, the fitting error is on the order of 1% for every simulation. Furthermore, we find that fitting error decreases with the magnitude of the remnant’s spin. This is likely because the QNMs decay faster as the spin magnitude decreases, which implies that more of the fit to the numerical waveform is influenced by numerical noise. As for the connection to the misalignment angle θ , precessing black hole binaries require less fine-tuning of their spin configurations to produce slowly-spinning remnants, since the spin of the progenitor black holes need not be aligned with the angular orbital momentum. In the future, it could be useful to perform fits which have a varying end time based on the magnitude of the remnant’s spin, but we save this for future work.

Appendix B: Parity Breaking Over the Remnant Equator

One way to quantify the asymmetry of the $\pm m$ QNMs is by looking at their behavior under the z -parity operation, which is defined to act on the strain such that

$$P_z(h_{(\ell,m)}) = (-1)^\ell \bar{h}_{(\ell,-m)}, \quad (\text{B1})$$

where the overbar denotes a complex conjugate. We can quantify the overall parity violation in the superrest

frame by computing

$$P = \sqrt{\frac{\sum_{\ell,m} |h_{(\ell,m)} - (-1)^\ell \bar{h}_{(\ell,-m)}|^2}{4 \sum_{\ell,m} |h_{(\ell,m)}|^2}}, \quad (\text{B2})$$

as described in [60]. For non-precessing simulations, P will be zero, up to numerical noise. However, precessing systems can exhibit significant parity breaking in the $\pm m$ QNMs.

In Fig. 7 we show the parity violation of all the simulations in our catalog. The non-precessing systems are clearly separated from the precessing systems, as denoted by the vertical axis break. Note that there are many precessing systems which have a remnant spin misalignment angle $\theta \approx 0$ or π . Remnant spin misalignment is not strictly required in precessing systems: fine-tuning of the spins, such as is found in superkick configurations [83] for example, can allow for precessing systems with $\theta \approx 0$, and large mass ratio systems can have essentially arbitrary θ .

-
- [1] S. A. Teukolsky, *Astrophys. J.* **185**, 635 (1973).
 - [2] A. Buonanno, G. B. Cook, and F. Pretorius, *Phys. Rev. D* **75**, 124018 (2007), arXiv:gr-qc/0610122.
 - [3] R. Owen, *Phys. Rev. D* **80**, 084012 (2009), arXiv:0907.0280 [gr-qc].
 - [4] N. Andersson, *Journal of Astrophysics and Astronomy* **20**, 269 (1999).
 - [5] V. P. Frolov and I. D. Novikov, eds., *Black hole physics: Basic concepts and new developments* (Springer, 1998).
 - [6] C. V. Vishveshwara, *Phys. Rev. D* **1**, 2870 (1970).
 - [7] W. H. Press, *Astrophys. J. Lett.* **170**, L105 (1971).
 - [8] S. Chandrasekhar and S. L. Detweiler, *Proc. Roy. Soc. Lond. A* **344**, 441 (1975).
 - [9] E. W. Leaver, *Proc. Roy. Soc. Lond. A* **402**, 285 (1985).
 - [10] S. L. Detweiler, *Astrophys. J.* **239**, 292 (1980).
 - [11] E. Berti and V. Cardoso, *Phys. Rev. D* **74**, 104020 (2006).
 - [12] E. W. Leaver, *Phys. Rev. D* **34**, 384 (1986).
 - [13] I. Kamaretsos, M. Hannam, and B. Sathyaprakash, *Phys. Rev. Lett.* **109**, 141102 (2012), arXiv:1207.0399 [gr-qc].
 - [14] I. Kamaretsos, M. Hannam, S. Husa, and B. S. Sathyaprakash, *Phys. Rev. D* **85**, 024018 (2012).
 - [15] L. London, *Phys. Rev. D* **102**, 084052 (2020).
 - [16] X. Li, L. Sun, R. K. L. Lo, E. Payne, and Y. Chen, *Phys. Rev. D* **105**, 024016 (2022).
 - [17] S. Borhanian, K. G. Arun, H. P. Pfeiffer, and B. S. Sathyaprakash, *Class. Quant. Grav.* **37**, 065006 (2020), arXiv:1901.08516 [gr-qc].
 - [18] X. Jiménez Forteza, S. Bhagwat, P. Pani, and V. Ferrari, *Phys. Rev. D* **102**, 044053 (2020).
 - [19] L. London, D. Shoemaker, and J. Healy, *Phys. Rev. D* **90**, 124032 (2014), [Erratum: *Phys. Rev. D* **94**, 069902 (2016)], arXiv:1404.3197 [gr-qc].
 - [20] D. Gangardt, N. Steinle, M. Kesden, D. Gerosa, and E. Stoikos, *Phys. Rev. D* **103**, 124026 (2021).
 - [21] T. A. Apostolatos, C. Cutler, G. J. Sussman, and K. S. Thorne, *Phys. Rev. D* **49**, 6274 (1994).
 - [22] L. E. Kidder, *Phys. Rev. D* **52**, 821 (1995).
 - [23] A. Buonanno, Y.-b. Chen, and M. Vallisneri, *Phys. Rev. D* **67**, 104025 (2003), [Erratum: *Phys. Rev. D* **74**, 029904 (2006)], arXiv:gr-qc/0211087.
 - [24] A. Apte and S. A. Hughes, *Phys. Rev. D* **100**, 084031 (2019).
 - [25] H. Lim, G. Khanna, A. Apte, and S. A. Hughes, *Phys. Rev. D* **100**, 084032 (2019), arXiv:1901.05902 [gr-qc].
 - [26] S. A. Hughes, A. Apte, G. Khanna, and H. Lim, *Phys. Rev. Lett.* **123**, 161101 (2019), arXiv:1901.05900 [gr-qc].
 - [27] S. Ghosh, P. Kolitsidou, and M. Hannam, arXiv eprints (2023), arXiv:2310.16980 [gr-qc].
 - [28] V. Ferrari and B. Mashhoon, *Phys. Rev. D* **30**, 295 (1984).
 - [29] B. Mashhoon, *Phys. Rev. D* **31**, 290 (1985).
 - [30] S. R. Dolan, *Phys. Rev. D* **82**, 104003 (2010), arXiv:1007.5097 [gr-qc].
 - [31] H. Yang, D. A. Nichols, F. Zhang, A. Zimmerman, Z. Zhang, and Y. Chen, *Phys. Rev. D* **86**, 104006 (2012), arXiv:1207.4253 [gr-qc].
 - [32] S. Hadar, D. Kapec, A. Lupasca, and A. Strominger, *Class. Quant. Grav.* **39**, 215001 (2022), arXiv:2205.05064 [gr-qc].
 - [33] P. Schmidt, M. Hannam, and S. Husa, *Phys. Rev. D* **86**, 104063 (2012), arXiv:1207.3088 [gr-qc].
 - [34] R. O’Shaughnessy, L. London, J. Healy, and D. Shoemaker, *Phys. Rev. D* **87**, 044038 (2013), arXiv:1209.3712 [gr-qc].
 - [35] M. Boyle, R. Owen, and H. P. Pfeiffer, *Phys. Rev. D* **84**, 124011 (2011).
 - [36] Y. Pan, A. Buonanno, A. Taracchini, L. E. Kidder, A. H. Mroué, H. P. Pfeiffer, M. A. Scheel, and B. Szilá-

- gyi, *Phys. Rev. D* **89**, 084006 (2014), arXiv:1307.6232 [gr-qc].
- [37] E. Hamilton, L. London, and M. Hannam, *Phys. Rev. D* **107**, 104035 (2023), arXiv:2301.06558 [gr-qc].
- [38] S. Babak, A. Taracchini, and A. Buonanno, *Phys. Rev. D* **95**, 024010 (2017), arXiv:1607.05661 [gr-qc].
- [39] S. Ossokine *et al.*, *Phys. Rev. D* **102**, 044055 (2020), arXiv:2004.09442 [gr-qc].
- [40] A. Ramos-Buades, A. Buonanno, M. Khalil, and S. Ossokine, *Phys. Rev. D* **105**, 044035 (2022), arXiv:2112.06952 [gr-qc].
- [41] M. Giesler, M. Isi, M. A. Scheel, and S. Teukolsky, *Phys. Rev. X* **9**, 041060 (2019), arXiv:1903.08284 [gr-qc].
- [42] E. Finch and C. J. Moore, *Phys. Rev. D* **103**, 084048 (2021), arXiv:2102.07794 [gr-qc].
- [43] K. Mitman *et al.*, *Phys. Rev. D* **104**, 024051 (2021), arXiv:2105.02300 [gr-qc].
- [44] L. Magaña Zertuche *et al.*, *Phys. Rev. D* **105**, 104015 (2022), arXiv:2110.15922 [gr-qc].
- [45] K. Mitman *et al.*, *Phys. Rev. D* **106**, 084029 (2022), arXiv:2208.04356 [gr-qc].
- [46] L. Gualtieri, E. Berti, V. Cardoso, and U. Sperhake, *Phys. Rev. D* **78**, 044024 (2008), arXiv:0805.1017 [gr-qc].
- [47] J. Aasi *et al.* (LIGO Scientific), *Class. Quant. Grav.* **32**, 074001 (2015), arXiv:1411.4547 [gr-qc].
- [48] F. Acernese *et al.* (VIRGO), *Class. Quant. Grav.* **32**, 024001 (2015), arXiv:1408.3978 [gr-qc].
- [49] T. Akutsu *et al.* (KAGRA), *PTEP* **2021**, 05A101 (2021), arXiv:2005.05574 [physics.ins-det].
- [50] M. Boyle *et al.*, *Class. Quant. Grav.* **36**, 195006 (2019), arXiv:1904.04831 [gr-qc].
- [51] J. Mac Uilliam, S. Akçay, and J. E. Thompson, *Phys. Rev. D* **109**, 084077 (2024), arXiv:2402.06781 [gr-qc].
- [52] A. Dhani, S. Völkel, A. Buonanno, H. Estelles, J. Gair, H. P. Pfeiffer, L. Pompili, and A. Toubiana, (2024), arXiv:2404.05811 [gr-qc].
- [53] https://github.com/HengruiPrinceton/precession_ringdown (2024).
- [54] M. Isi and W. M. Farr, arXiv eprints (2021), arXiv:2107.05609 [gr-qc].
- [55] N. Deppe, W. Throwe, L. E. Kidder, N. L. Vu, K. C. Nelli, C. Armaza, M. S. Bonilla, F. Hébert, Y. Kim, P. Kumar, G. Lovelace, A. Macedo, J. Moxon, E. O'Shea, H. P. Pfeiffer, M. A. Scheel, S. A. Teukolsky, N. A. Wittek, *et al.*, *SpECTRE v2023.10.11*, 10.5281/zenodo.8431874 (2023).
- [56] J. Moxon, M. A. Scheel, and S. A. Teukolsky, *Phys. Rev. D* **102**, 044052 (2020), arXiv:2007.01339 [gr-qc].
- [57] J. Moxon, M. A. Scheel, S. A. Teukolsky, N. Deppe, N. Fischer, F. Hébert, L. E. Kidder, and W. Throwe, *Phys. Rev. D* **107**, 064013 (2023), arXiv:2110.08635 [gr-qc].
- [58] M. Boyle, D. Iozzo, and L. C. Stein, *moble/scrivi*: v1.2 (2020).
- [59] M. Boyle, *Phys. Rev. D* **87**, 104006 (2013).
- [60] M. Boyle, L. E. Kidder, S. Ossokine, and H. P. Pfeiffer, Gravitational-wave modes from precessing black-hole binaries (2014), arXiv:1409.4431 [gr-qc].
- [61] M. Boyle, *Phys. Rev. D* **93**, 084031 (2016), arXiv:1509.00862 [gr-qc].
- [62] E. Berti and A. Klein, *Phys. Rev. D* **90**, 064012 (2014), arXiv:1408.1860 [gr-qc].
- [63] H. Zhu, J. L. Ripley, A. Cárdenas-Avenidaño, and F. Pretorius, arXiv eprints (2023), arXiv:2309.13204 [gr-qc].
- [64] L. T. London, *Phys. Rev. D* **102**, 084052 (2020), arXiv:1801.08208 [gr-qc].
- [65] S. Bhagwat, X. J. Forteza, P. Pani, and V. Ferrari, *Phys. Rev. D* **101**, 044033 (2020), arXiv:1910.08708 [gr-qc].
- [66] V. Baibhav, M. H.-Y. Cheung, E. Berti, V. Cardoso, G. Carullo, R. Cotesta, W. Del Pozzo, and F. Duque, arXiv e-prints (2023), arXiv:2302.03050 [gr-qc].
- [67] M. H.-Y. Cheung, E. Berti, V. Baibhav, and R. Cotesta, arXiv e-prints (2023), arXiv:2310.04489 [gr-qc].
- [68] M. Ruiz, R. Takahashi, M. Alcubierre, and D. Nunez, *Gen. Rel. Grav.* **40**, 2467 (2008), arXiv:0707.4654 [gr-qc].
- [69] D. A. B. Iozzo *et al.*, *Phys. Rev. D* **103**, 124029 (2021), arXiv:2104.07052 [gr-qc].
- [70] M. Boyle, *Journal of Mathematical Physics* **57**, 092504 (2016), https://pubs.aip.org/aip/jmp/article-pdf/doi/10.1063/1.4962723/13685223/092504_1_online.pdf.
- [71] E. Wigner, *Group theory: And its application to the quantum mechanics of atomic spectra* (2012).
- [72] P. Schmidt, M. Hannam, S. Husa, and P. Ajith, *Phys. Rev. D* **84**, 024046 (2011).
- [73] W. H. Press and S. A. Teukolsky, *Astrophys. J.* **185**, 649 (1973).
- [74] E. Berti, V. Cardoso, and C. M. Will, *Phys. Rev. D* **73**, 064030 (2006), arXiv:gr-qc/0512160.
- [75] E. Berti, V. Cardoso, J. A. Gonzalez, U. Sperhake, M. Hannam, S. Husa, and B. Bruegmann, *Phys. Rev. D* **76**, 064034 (2007), arXiv:gr-qc/0703053.
- [76] E. Berti, V. Cardoso, J. A. Gonzalez, U. Sperhake, and B. Bruegmann, *Class. Quant. Grav.* **25**, 114035 (2008), arXiv:0711.1097 [gr-qc].
- [77] M. Davis, R. Ruffini, and J. Tiomno, *Phys. Rev. D* **5**, 2932 (1972).
- [78] A. Le Tiec and L. Blanchet, *Class. Quant. Grav.* **27**, 045008 (2010), arXiv:0910.4593 [gr-qc].
- [79] R. O'Shaughnessy, B. Vaishnav, J. Healy, Z. Meeks, and D. Shoemaker, *Phys. Rev. D* **84**, 124002 (2011), arXiv:1109.5224 [gr-qc].
- [80] J. D. Schnittman, A. Buonanno, J. R. van Meter, J. G. Baker, W. D. Boggs, J. Centrella, B. J. Kelly, and S. T. McWilliams, *Phys. Rev. D* **77**, 044031 (2008), arXiv:0707.0301 [gr-qc].
- [81] W. B. Bonnor and M. A. Rotenberg, *Proceedings of the Royal Society of London Series A* **265**, 109 (1961).
- [82] B. Brüggmann, J. A. González, M. Hannam, S. Husa, and U. Sperhake, *Phys. Rev. D* **77**, 124047 (2008).
- [83] S. Ma, M. Giesler, V. Varma, M. A. Scheel, and Y. Chen, *Phys. Rev. D* **104**, 084003 (2021), arXiv:2107.04890 [gr-qc].
- [84] F. Alessio and M. Arzano, *Journal of High Energy Physics* **2019**, 28 (2019).
- [85] F. Pretorius, arXiv e-prints (2007), arXiv:0710.1338 [gr-qc].
- [86] D. Keppel, D. A. Nichols, Y. Chen, and K. S. Thorne, *Phys. Rev. D* **80**, 124015 (2009), arXiv:0902.4077 [gr-qc].
- [87] D. Gerosa and C. J. Moore, *Phys. Rev. Lett.* **117**, 011101 (2016), arXiv:1606.04226 [gr-qc].
- [88] S. Marsat and J. G. Baker, arXiv e-prints (2018), arXiv:1806.10734 [gr-qc].
- [89] R. Gamba, S. Akçay, S. Bernuzzi, and J. Williams, *Phys. Rev. D* **106**, 024020 (2022), arXiv:2111.03675 [gr-qc].
- [90] S. Ossokine, A. Buonanno, S. Marsat, R. Cotesta,

- S. Babak, T. Dietrich, R. Haas, I. Hinder, H. P. Pfeiffer, M. Pürrer, C. J. Woodford, M. Boyle, L. E. Kidder, M. A. Scheel, and B. Szilágyi, *Phys. Rev. D* **102**, 044055 (2020).
- [91] A. Ramos-Buades, A. Buonanno, H. Estellés, M. Khalil, D. P. Mihaylov, S. Ossokine, L. Pompili, and M. Shiferaw, *Phys. Rev. D* **108**, 124037 (2023).
- [92] H. Estellés, M. Colleoni, C. García-Quirós, S. Husa, D. Keitel, M. Mateu-Lucena, M. d. L. Planas, and A. Ramos-Buades, *Phys. Rev. D* **105**, 084040 (2022), [arXiv:2105.05872 \[gr-qc\]](#).
- [93] J. E. Thompson, E. Hamilton, L. London, S. Ghosh, P. Kolitsidou, C. Hoy, and M. Hannam, *Phys. Rev. D* **109**, 063012 (2024), [arXiv:2312.10025 \[gr-qc\]](#).
- [94] E. Hamilton, L. London, J. E. Thompson, E. Fauchon-Jones, M. Hannam, C. Kalaghatgi, S. Khan, F. Pannarale, and A. Vano-Vinuales, *Phys. Rev. D* **104**, 124027 (2021).
- [95] S. Babak, A. Taracchini, and A. Buonanno, *Phys. Rev. D* **95**, 024010 (2017).
- [96] G. Carullo, W. Del Pozzo, and J. Veitch, *Phys. Rev. D* **99**, 123029 (2019), [Erratum: *Phys. Rev. D* **100**, 089903 (2019)], [arXiv:1902.07527 \[gr-qc\]](#).
- [97] M. Isi, M. Giesler, W. M. Farr, M. A. Scheel, and S. A. Teukolsky, *Phys. Rev. Lett.* **123**, 111102 (2019), [arXiv:1905.00869 \[gr-qc\]](#).
- [98] R. Cotesta, G. Carullo, E. Berti, and V. Cardoso, *Phys. Rev. Lett.* **129**, 111102 (2022), [arXiv:2201.00822 \[gr-qc\]](#).
- [99] M. Crisostomi, K. Dey, E. Barausse, and R. Trotta, *Phys. Rev. D* **108**, 044029 (2023), [arXiv:2305.18528 \[gr-qc\]](#).
- [100] V. Gennari, G. Carullo, and W. Del Pozzo, *arXiv e-prints* (2023), [arXiv:2312.12515 \[gr-qc\]](#).
- [101] A. Correia, Y.-F. Wang, and C. D. Capano, *arXiv e-prints* (2023), [arXiv:2312.14118 \[gr-qc\]](#).
- [102] M. Isi and W. M. Farr, *Phys. Rev. Lett.* **131**, 169001 (2023).
- [103] G. Carullo, R. Cotesta, E. Berti, and V. Cardoso, *Phys. Rev. Lett.* **131**, 169002 (2023).
- [104] E. Finch and C. J. Moore, *Phys. Rev. D* **106**, 043005 (2022), [arXiv:2205.07809 \[gr-qc\]](#).
- [105] Y.-F. Wang, C. D. Capano, J. Abedi, S. Kastha, B. Krishnan, A. B. Nielsen, A. H. Nitz, and J. Westerweck, *arXiv e-prints* (2023), [arXiv:2310.19645 \[gr-qc\]](#).
- [106] S. Ma, L. Sun, and Y. Chen, *Phys. Rev. D* **107**, 084010 (2023), [arXiv:2301.06639 \[gr-qc\]](#).
- [107] H.-T. Wang and L. Shao, *Phys. Rev. D* **108**, 123018 (2023), [arXiv:2311.13300 \[gr-qc\]](#).
- [108] M. Isi and W. M. Farr, *arXiv e-prints* (2022), [arXiv:2202.02941 \[gr-qc\]](#).
- [109] J. Calderón Bustillo, P. D. Lasky, and E. Thrane, *Phys. Rev. D* **103**, 024041 (2021), [arXiv:2010.01857 \[gr-qc\]](#).
- [110] R. Abbott *et al.* (LIGO Scientific, Virgo), *Astrophys. J. Lett.* **900**, L13 (2020), [arXiv:2009.01190 \[astro-ph.HE\]](#).
- [111] C. D. Capano, M. Cabero, J. Westerweck, J. Abedi, S. Kastha, A. H. Nitz, Y.-F. Wang, A. B. Nielsen, and B. Krishnan, *Phys. Rev. Lett.* **131**, 221402 (2023), [arXiv:2105.05238 \[gr-qc\]](#).
- [112] R. Abbott *et al.* (LIGO Scientific Collaboration and Virgo Collaboration), *Phys. Rev. D* **103**, 122002 (2021).
- [113] H. Siegel, M. Isi, and W. M. Farr, *Phys. Rev. D* **108**, 064008 (2023), [arXiv:2307.11975 \[gr-qc\]](#).
- [114] R. Abbott, T. D. Abbott, S. Abraham, F. Acernese, K. Ackley, C. Adams, R. X. Adhikari, V. B. Adya, C. Affeldt, M. Agathos, *et al.*, *Phys. Rev. Lett.* **125**, 101102 (2020), [arXiv:2009.01075 \[gr-qc\]](#).
- [115] V. Varma, S. E. Field, M. A. Scheel, J. Blackman, D. Gerosa, L. C. Stein, L. E. Kidder, and H. P. Pfeiffer, *Phys. Rev. Research* **1**, 033015 (2019), [arXiv:1905.09300 \[gr-qc\]](#).
- [116] M. L. Waskom, *Journal of Open Source Software* **6**, 3021 (2021).
- [117] J. D. Hunter, *Computing in Science & Engineering* **9**, 90 (2007).
- [118] T. Kluyver *et al.*, *Jupyter notebooks – a publishing format for reproducible computational workflows* (2016).
- [119] C. R. Harris *et al.*, *Nature* **585**, 357 (2020).
- [120] G. Van Rossum and F. L. Drake, *Python 3 Reference Manual* (CreateSpace, Scotts Valley, CA, 2009).